View metadata, citation and similar papers at core.ac.uk

brought to you by CORE

provided by Nottingham ePrints

Starr, Nichola J. and Johnson, Daniel J. and Wibawa, Judata and Marlow, Ian and Bell, Mike and Barrett, David A. and Scurr, David J. (2016) Age-related changes to human stratum corneum lipids detected using time-of-flight secondary ion mass spectrometry following in vivo sampling. Analytical Chemistry, 88 . pp. 4400-4408. ISSN 1520-6882

Access from the University of Nottingham repository:
http://eprints.nottingham.ac.uk/33074/1/Starr%20et%20al_UoN%20Repository%20File.pdf

Copyright and reuse:

The Nottingham ePrints service makes this work by researchers of the University of Nottingham available open access under the following conditions.

This article is made available under the Creative Commons Attribution Non-commercial licence and may be reused according to the conditions of the licence. For more details see: http://creativecommons.org/licenses/by-nc/2.5/

A note on versions:

The version presented here may differ from the published version or from the version of record. If you wish to cite this item you are advised to consult the publisher's version. Please see the repository url above for details on accessing the published version and note that access may require a subscription.

For more information, please contact eprints@nottingham.ac.uk

Age-Related Changes to Human *Stratum Corneum* Lipids Detected Using ToF-SIMS Following *in Vivo* Sampling

Nichola J. Starr[§], Daniel J. Johnson[†], Judata Wibawa[‡], Ian Marlow[‡], Mike Bell[‡], David A. Barrett[§], David J. Scurr*[§]

[§] School of Pharmacy, University of Nottingham, Nottingham, NG7 2RD, UK

[†] College of Engineering, Swansea University, Swansea, SA1 8EN, UK

[‡] Walgreens Boots Alliance, Thane Road, Nottingham, NG90 1BS, UK

ABSTRACT: This work demonstrates the ability to detect changes in both quantity and spatial distribution of human *stratum corneum* (*SC*) lipids from samples collected *in vivo*. The *SC* functions as the predominant barrier to the body, protecting against the penetration of xenobiotic substances. Changes to the *SC* lipid composition have been associated with barrier impairment and consequent skin disorders and it is therefore important to monitor and quantify changes to this structure. This work demonstrates the first reported use of time of flight secondary ion mass spectrometry (ToF-SIMS) to assess physiological changes to human *SC* as a function of depth. This technique provides exceptional sensitivity and chemical specificity, allowing analysis of single tape stripped samples taken from volunteers. Using this methodology we were able to successfully identify chemical differences in human *SC* resulting from both intrinsic and extrinsic (photo) aging. Samples were collected from women of two age groups (under 27 and post-menopausal) and from two body sites with varying UV exposure (inner forearm and dorsal hand) and differences were identified using multivariate data analysis. The key finding was the significant aged-related increase and change in spatial distribution of the sterol cholesterol sulfate, a membrane stabilizing lipid. Significant changes in the prevalence of both lignoceric acid (C24:0) and hexacosanoic acid (C26:0) were also observed. This work describes previously unreported age-related chemical changes to human *SC*, providing an insight into aging mechanisms which may improve the design of both pharmaceutical and cosmetic topical products.

The *stratum corneum* consists of tightly stacked layers of corneocytes surrounded by an intercellular lipid-rich domain and despite being only 10-20 μm thick it provides the primary barrier to the body, preventing transepidermal water loss and the penetration of xenobiotic substances.[1] Although previously thought to be a metabolically inert structure, the role of the *SC* as a natural biosensor is now known to be crucial in the defence mechanism of the skin.[2] Examples include changes to external humidity which initiate filaggrin proteolysis and the release of preformed cytokines to regulate epidermal lipid synthesis in response to acute barrier disruption.[2] Changes in the *SC* lipid composition have also been linked to various skin disorders, including atopic dermatitis, psoriasis and ichthyoses, reviewed by Harding[3] and more recently Jungersted and Agner.[4] Detailed chemical analysis of this tissue and the changes it undergoes in response to both internal and external factors is therefore hugely important in order to facilitate more effective skin treatments.

Time of flight secondary ion mass spectrometry (ToF-SIMS) is a surface analysis technique that provides high chemical sensitivity and specificity. Successful analysis of a wide range of biological compounds have been demonstrated using ToF-SIMS, including proteins[5] and lipids[6] from a variety of biological substrates, including bacteria[7], individual cells[8] and both healthy[9] and diseased tissue[10]. ToF-SIMS analysis has recently been employed to monitor permeation of topically applied compounds through *ex vivo* skin tissue, both animal [11] and human[12]. However, this technique has not yet been utilised to study the lipid composition of native human skin, despite offering several advantages over traditionally used chromatographic mass spectrometry methods. ToF-SIMS requires no prior sample preparation except the removal of excess moisture, which allows biological samples to be analysed in their original state without the need for a dissolution or extraction process. The technique can also simultaneously detect ions from multiple components within a sample, eliminating the need for the often complicated separation step found in chromatographic methods. However, the key advantage offered by ToF-SIMS is the ability to map the spatial distribution of detected ions within a sample, with a resolution of 1 μm achievable.

The lipid composition of the *SC* is unique and significantly different to other biological membranes. Typical keratinocyte plasma membranes contain high levels of phospholipids yet the *SC* contains virtually none, as depletion of these lipids accompanies cornification.[13] Instead this tissue consists predominantly of three main species, ceramides, cholesterol and fatty acids, in an equimolar ratio.[1] Cholesterol sulfate is also present in small quantities, declining from 5% of the total lipid content in the underlying layers of the *SC* to only 1% in the most superficial layers.[14] Despite this, it has emerged as a significantly important component with Sato *et al.* proposing that it plays a role in regulating desquamation, through inhibition of proteases which facilitate corneocyte loss.[15] Elias *et al.* had previously demonstrated a fivefold increase in this molecule in patients with recessive X-linked ichthyosis.[16] This hereditary

condition results from a deficiency in steroid sulfatase and causes extreme scaling of the skin and both Elias *et al.*[17] and Sato *et al.*[15] have induced scaling of murine skin through topical cholesterol sulfate application. It is also known that this sterol is found in keratinizing membranes at much higher levels than in mucosal membranes, further supporting the suggestion that it is involved the regulation of desquamation.[14]

Research into aging skin is becoming increasingly popular, a consequence of both an aging population and an increased awareness of UV damage. The aging process in skin occurs through two pathways, intrinsic and extrinsic.[18] Intrinsic aging is a consequence of the degenerative process the body undergoes over time, whereas extrinsic aging becomes apparent in people from a much younger age due to exposure to environmental factors, such as cigarette smoke, pollution and UV radiation.[18] Prolonged exposure to UV radiation in particular can result in phenotypic changes, an effect termed photo damage.[18] The majority of research surrounding aging skin is focused on changes to physical parameters, such as transepidermal water loss, surface pH or skin hydration.[19] However, information regarding age-related changes to the *SC* lipid composition is less documented and different groups have reported variable effects. Both Jungersted *et al.*[4] and Imokawa *et al.*[20] used the cyanoacrylate method to remove human *SC* and conducted analysis using thin layer chromatography. Yet while Jungersted *et al.*[4] noted no significant change in any of the individual ceramide classes, Imokawa et al.[20] reported a significant decrease in total ceramide content with age. Rogers *et al.*[21] also used thin layer chromatography to report an age-related decrease in all three major lipid classes, but this analysis was conducted using pooled tape stripped samples. Denda *et al.*[22] used solvent extraction coupled with thin layer chromatography to reveal both an increase and decrease in individual ceramide classes, but only in female volunteers. There is also limited information regarding the effect of environmental exposure on *SC* lipids. Bak *et al.*[23] demonstrated a significant decrease in murine *SC* ceramide content following long term UV exposure and Boireau-Adamezyk *et al.*[24] reported a decrease in cholesterol levels when comparing an exposed arm site to a protected one. Despite its proposed importance in desquamation, only one group to date have focused on a change in cholesterol sulfate levels with age. Haratake *et al.*[25] conducted thin layer chromatographic analysis of extracted lipids from murine *SC* to demonstrate that cholesterol sulfate and cholesterol levels were increased and decreased respectively in aged mice.

Despite the presence of a lipid gradient within the *SC*[26] there is limited research assessing both lipid composition in general and age-related changes as a function of *SC* depth. Typical *SC* sampling methods, such as surface extraction and cyanoacrylate resin, sample the *SC* as a whole and until recently instrument sensitivity required sequential tape strips to be pooled. Both Egawa *et al.*[27] and Boireau-Adamezyk *et al.*[24] have recently demonstrated the ability to record measurements at varying depths within the *SC in vivo* using Raman spectroscopy, at depths of 2 and 4 μm apart respectively. However, this technique cannot provide the chemical specificity that is offered by mass spectrometry techniques.

This study describes the first reported application of ToF-SIMS to conduct chemical analysis of native human *SC* from individual tape stripped samples collected *in vivo*. In addition to exceptional sensitivity and chemical specificity, ToF-SIMS also allows the spatial distribution of compounds to be mapped. Therefore, by combining ToF-SIMS with tape stripping both the composition and distribution of lipids can be monitored as a function of *SC* depth.

EXPERIMENTAL SECTION

Sample Population. The sample population consisted of healthy female volunteers with a Fitzpatrick skin type II/III.[28] In order to observe differences due to intrinsic aging, samples were taken from 9 females under 27 years old and 9 post-menopausal females (typically > 60 years of age). In order to observe differences caused by extrinsic aging, samples were collected from both the flexor forearm (low UV exposure) and dorsal hand (high UV exposure) for each volunteer. For the purpose of this study the following abbreviations will be used: post-menopausal (old or O), under 27 year old (young or Y), arm (A) and hand (H). All volunteers participated after providing consent and confirmed they were free from skin conditions, medication and had not recently used any form of artificial tanning methods.

Sample Collection. Tape stripping experiments were performed using D-Squame® skin sampling discs (CuDerm, Dallas, Tx, USA). The circular discs had a diameter of 22 mm and used a fully cured medical grade synthetic poly-acrylate ester adhesive. The disc was applied to the skin, a constant pressure applied using a pressure disc applicator (CuDerm) and the disc removed in one fluent motion. Fifteen consecutive tape strips were taken per body site for each volunteer. The tape strip data reported in this study are specified as strip 1 being the uppermost layer and strip 15 being the deepest. Samples were stored at -18 °C until required for analysis. Prior to analysis samples were attached to glass slides and vacuum dried at 40 °C for 20 minutes.

Scanning electron microscopy (SEM). Analysis was conducted on tape strip no. 6 for three volunteers from each age category. Tape strip 6 was chosen due to its median position within the collected samples. The tape stripped samples were mounted onto aluminum SEM stubs of 12.5 mm diameter, using carbon based, electrically conductive, double sided adhesive discs as the mounting adhesive. Prior to analysis the samples were sputter coated with gold for 3 minutes resulting in a surface coverage of approximately 20 nm. The samples were analysed using a Jeol 6060LV Variable Pressure SEM in high vacuum mode, using a range of spot sizes and voltages to optimise the individual sample resolution. Samples were imaged at × 800 magnification.

Atomic force microscopy (AFM). Analysis was conducted on samples from one volunteer from each age category with each alternate tape strip (strip 2 - 14) analysed. AFM measurements were performed on a Multimode AFM with NanoScope IIIa controller (Bruker, USA) using manufacturer supplied software. All measurements were carried out using tapping mode under ambient laboratory conditions (humidity ~60 %, temperature ~22 °C) using TESP probes (nominal spring constant 20-80 N/m). Data was analysed using instrument control software (NanoScope software version 5.31R1 was used throughout). Tape stripped samples were fixed to metal sample stubs prior to imaging. For sample height measurements, images were taken with approximately equal areas of skin and substrate visible. Line profiles were then taken across the surface and the maximum height of the corneocyte layer above the substrate plane was measured. Three images

were taken from different areas of each sample, with three line profiles taken from each image, making all step height values quoted as the mean of nine individual measurements.

Time of flight secondary ion mass spectrometry (ToF-SIMS). Analysis was performed using a ToF-SIMS IV instrument (IONTOF, GmbH) with a Bi_3^+ cluster primary ion source and a single-stage reflectron analyser. A primary ion energy of 25 keV, a pulsed target current of approximately 0.3 pA and post-acceleration energy of 10 keV were employed throughout the analysis. The primary ion beam had a focused beam size of 1-2µm and the primary ion dose density was maintained at $< 1 \times 10^{12}$ ions per cm^2 throughout to ensure static conditions. Charge compensation of the sample was performed using a low energy (< 20 eV) electron flood gun. Spectra were acquired in high current bunched mode over 4 × 4 mm areas in both positive and negative polarity, at a resolution of 100 pixels/mm. Each 4 × 4 mm area was scanned using the macro-raster stage function, using a random raster pattern. 64 separate 0.5 × 0.5 mm patches were scanned, with 15 scans acquired per patch. ToF-SIMS data was acquired and analysed using SurfaceLab 6 software (IONTOF, GmbH). Retrospective data analysis allowed ions indicative of organic material (eg. CN^- and $C_3H_8O^+$) to be identified and these were used to threshold the data-sets, removing data from the adhesive tape material observed between fissures in the stripped skin. Each data-set was then divided into four smaller data-sets for analysis, each representing a 1 × 1 mm sample area. This produced a repeat of n = 4 for every sample. Following subtraction of the substrate data, peak intensities were normalised to the total ion count of the spectra.

Multivariate data analysis. Multivariate data analysis (MVA) has become an increasingly popular analysis tool in the field of ToF-SIMS, particularly for biological samples.[29] MVA was conducted using SIMCA-P software (Version 13.1, Umetrics, MKS Instruments Inc.). The data was exported as peak intensities which had been normalised to the total ion count of the spectra. It was then mean centered and Pareto scaled, which involves the division of each variable by the square root of its standard deviation. Separation of the data sets was initially viewed using principal component analysis (PCA) to provide an unsupervised model, but final analysis was conducted using the supervised method orthogonal partial least-squares discriminant analysis (OPLSDA) to enhance class separation. The data is presented as both score plots and loadings S plots. The scores plots visualise both the inter-class variance (y axis) and the between class variance (x axis). The S plots display loadings as a function of the magnitude of contribution to the variance (x axis) and the reliability of the ion as a biomarker (y axis). Ions with a low reliability value (p(corr)) are considered too close to the spectrum noise to be considered a reliable biomarker, with possible values between -1 and 1. For this study we adopted a p(corr) cut off value of ±0.5 and so will only consider an ion as a potential biomarker if it has a p(corr)[1] value in the range $0.5<p(corr)[1]<-0.5$. The models are evaluated using R^2 and Q^2 values. The R^2 value measures the goodness of fit of the model and the closer to 1 the value the more reliable the model. Whereas the Q^2 value indicates the predictability of the model, with values >0.5 considered acceptable. It is also important to produce R^2 and Q^2 values which are numerically close to prevent overfitting of the model.[30]

RESULTS AND DISCUSSION

The effects of aging on corneocyte morphology. It has been established that both intrinsic and extrinsic aging can have an effect on corneocyte morphology, in particular increasing and decreasing the surface area respectively.[18] To determine whether these physical aging effects could be visualised from the tape stripped layers collected in this study, SEM analysis was conducted. Images were taken from a single tape strip, an example of which is shown in Figure 1a, from three volunteers from each age category and image analysis was performed to quantify the corneocyte surface area for six different cells per sample. Figure 1b shows the average corneocyte surface area for each sample type. For both age categories, the hand corneocytes show a significantly decreased surface area compared to the corresponding arm samples, demonstrating that a decrease in surface area is related to UV exposure. There is also a significant increase in corneocyte surface area in the post-menopausal arm samples compared to the under 27 group. This highlights an increase in surface area related to intrinsic aging. Interestingly, the two opposing aging effects result in no significant difference between the hand samples of the two age groups. These trends in surface area agree with known aging effects and demonstrate that both intrinsic and extrinsic *SC* aging is evident in our individual tape stripped layers. This therefore validates the use of these samples to study the chemical effects of aging using ToF-SIMS.

The effects of aging on the depth of *SC* removed. In order to compare the chemical profile of individual tape stripped samples it was first essential to confirm that an equal depth into the *SC* was being analysed per sample type. AFM was therefore employed to quantify the average *SC* thickness per tape strip per sample type. Step height measurements were taken to quantify the thickness of the *SC* layer protruding above the adhesive tape material (Figure 1c). Due to the pressure applied when collecting a tape stripped sample, part of the removed *SC* layer is ultimately embedded into the adhesive material. Therefore the step height measurement does not provide an absolute value for the thickness of a removed *SC* layer. However, as the pressure disc applicator used ensures that a constant pressure is applied to all samples, it can be assumed that the amount of *SC* embedded in the adhesive is equal across all samples. Therefore, the step height value can provide an accurate comparison of thickness across different sample types. Alternate strip numbers between two and fourteen were analysed for one volunteer per age category. The depth per individual strip number can be found in the supplementary information (Figure S1). Figure 1d shows the average *SC* layer thickness for each sample type, demonstrating that for these samples no significant difference was observed between the four groups. This result indicates that any chemical differences seen from analysis of an individual tape stripped layer can be confidently attributed to actual physiological effects as opposed to a difference in sampling depth of the *SC*.

The effects of aging on the chemical composition of the *SC*. ToF-SIMS analysis was initially conducted on alternate strips from strip no. 1 – 15 for one volunteer per age category. Examination of this data demonstrated that various trends in ion intensity as a function of *SC* depth could be identified for all sample types. The fact that various conflicting trends can be identified within a single data set validates the methodology and confirms that any differences seen are phys-

iologically relevant and not merely experimental artefacts. More importantly, it confirms that subtle differences can be seen between individual tape stripped layers, as illustrated in Figure 3a.

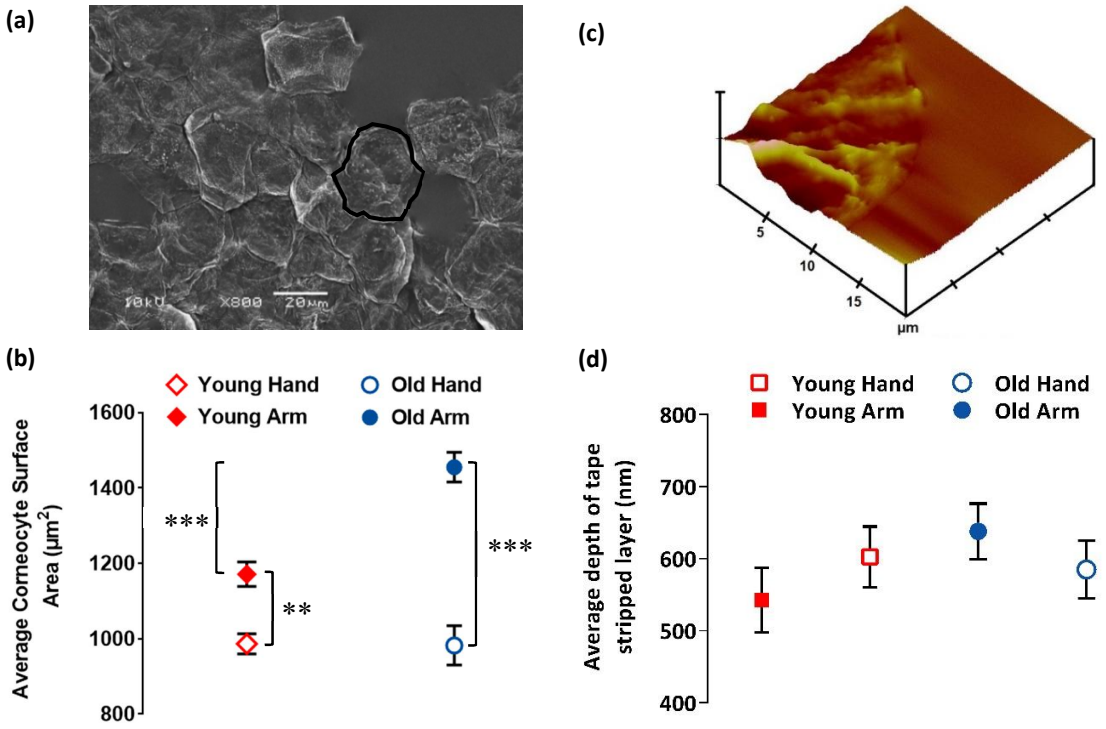

Figure 1. (a) An SEM image taken at ×800 magnification of one post-menopausal hand tape stripped sample. The black outline highlights an individual corneocyte. The scale bar represents 20µm. (b) Average corneocyte surface area per sample type, measured by SEM and image analysis. The data is shown as the mean and standard error calculated from n = 3 volunteers for each age group and n = 6 repeats for each sample. An unpaired, two tailed T test with Welch's correction was conducted on each sample pair (**** p value < 0.0001, *** p value < 0.001). (c) An example of an AFM step height image of a postmenopausal hand tape stripped sample taken over 20 × 20 µm. (d) Average thickness of *SC* layer removed per sample type, measured by AFM from one volunteer per sample type. The data is shown as the mean and standard error calculated from alternative strips (2-14) and n = 9 per strip. An unpaired, two tailed T test with Welch's correction was conducted on each sample pair but no significant difference was found.

In order to compare the chemical composition across all the volunteers, a single tape strip number was used for analysis. Due to its median position within the *SC* samples collected, tape strip 7 was chosen for cross-comparison, which should ensure that the chemical composition analysed does not include sebum surface lipids. The concentration of these lipids on the surface is highly variable between volunteers and largely depends on short-term environmental factors, such as the season[21], the lifestyle of the volunteer, in particular their diet[31] and most importantly age[32].

Due to the large number of peaks produced, differences between samples were initially identified using multivariate data analysis. PCA is a popular multivariate choice due to its unsupervised nature. However, this method only produces good class separation when the variation within a single class is sufficiently less than the variation between the two classes.[33] This poses a problem for biological data, in particular human samples, which suffer from significant variability between volunteers. It was therefore decided to use a supervised multivariate method, OPLSDA, which maximises class separation. PCA was used initially to view the data, followed by detailed OPLSDA analysis. The positive and negative polarity data were analysed independently. However, only the negative data was significantly split by the initial PCA (Figure S2) and so only this will be discussed. Four individual comparisons were made to assess both extrinsic aging (OA/OH and YA/YH) and intrinsic aging (OA/YA and OH/YH). The resulting scores and loadings plots for these four comparisons are shown in Figure 2. All four score plots show clear separation between classes, demonstrating that age-related changes to the *SC* were detected using ToF-SIMS. Importantly, these differences were detected from comparison of an individual tape strip. The loadings plots highlight which ions are responsible for this class separation. Ions with a p(corr)[1] value outside the range 0.5<p(corr)[1]<-0.5 were ignored due to poor reliability as a class marker. The loadings with the highest magnitude (p[1]) and hence highest contribution to the class variance which also

have a 0.5<p(corr)[1]<-0.5 are highlighted in the S plots and colour coded to demonstrate their class association.

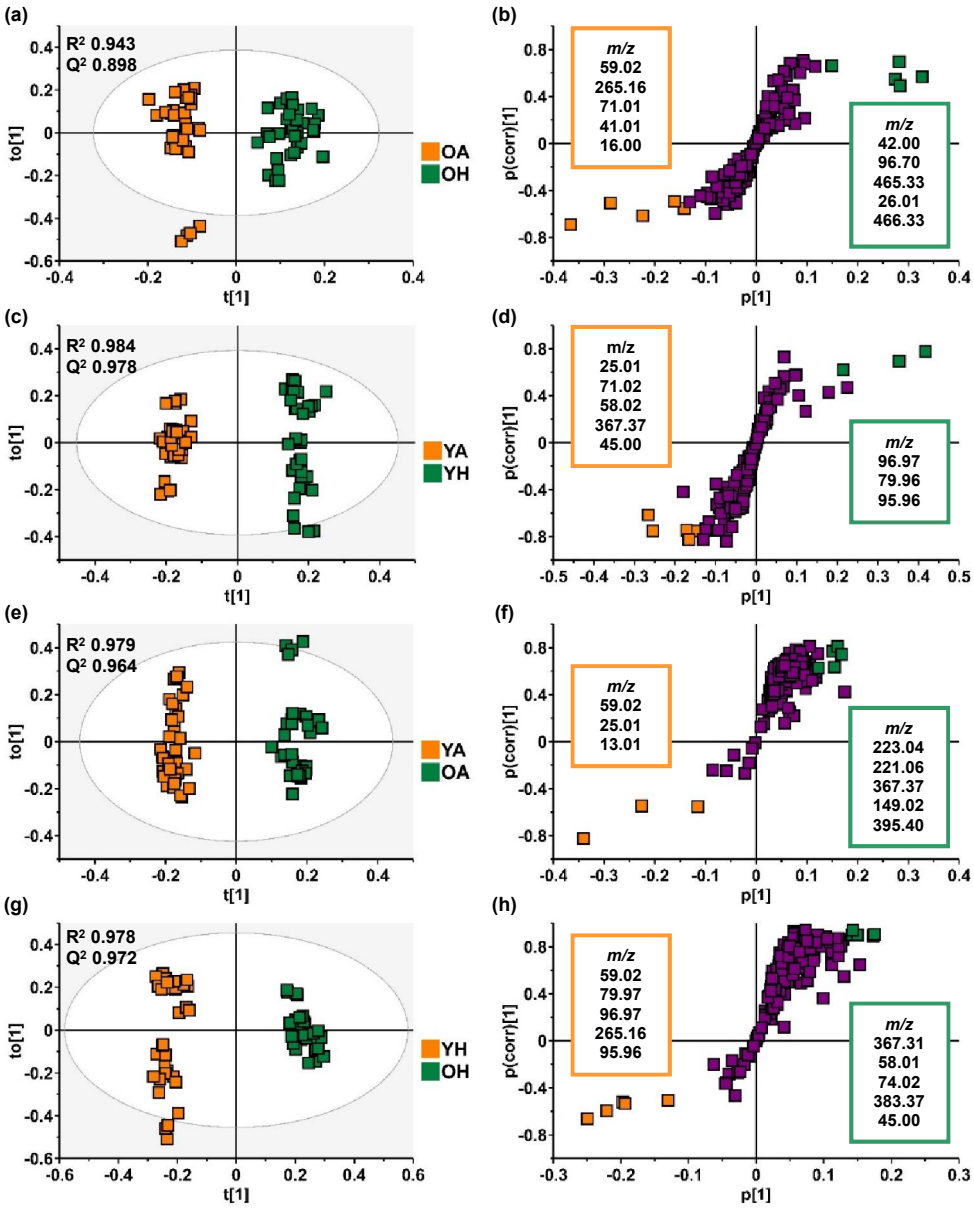

Figure 2. OPLSDA analysis of ToF-SIMS data which has been extracted from the spectra as normalised intensities (to total ion count). Score plots (a, c, e, g) and loadings S plots (b, d, f, h) are shown for the four aging comparisons. All comparisons produced models with good reliability (R^2 close to 1) and predictivity ($Q^2 > 0.5$). The loadings (ions with *m/z* values) that have the highest contribution to class variance with 0.5 <p(corr)[1]< -0.5 are highlighted in the S plots and colour coordinated to show which class they are associated with. Data was taken from tape strip number 7 for n = 9 volunteers per age category and n = 4 different measurements per volunteer.

Due to the similarity in structure of many *SC* lipids, the origin of many fragment ions could not be uniquely identified. Smaller ions (*m/z* <100) can be attributed to popular fragments which are abundant in biological tissue, such as CNO^- (*m/z* = 42), $C_2H_3O_2^-$ (*m/z* = 59) and an ion with *m/z* = 97 that could be assigned to either SO_4H^- or $H_2PO_4^-$. However, the loadings did highlight ions that could be attributed to the $[M-H]^-$ molecular markers of several *SC* lipids. Peaks with *m/z* = 367 and 395 correspond to the $[M-H]^-$ ions of two saturated fatty acids, lignoceric acid (C24:0) and hexacosanoic acid (C26:0) respectively. The endogenous fatty acid fraction of the *SC* has been characterized by Norlén *et al* as "a stable population with low interindividual variation, dominated by saturated lignoceric and hexacosanoic acid".[34] It is therefore not surprising that

these two fatty acids, above others, show variance between the different classes. These peaks are not highlighted as the highest contributors to class variance in all of the loadings plots. However, they demonstrate both good reliability as a biomarker ($0.5<p(corr)[1]<-0.5$) (Figure S3) and a statistically significant difference in peak intensity between classes (p value <0.05) (Figure S4). Interestingly these fatty acid peaks show opposite trends for intrinsic and extrinsic aging. They show an increase in intensity when comparing the post-menopausal samples to the under 27 samples, suggesting an increase in fatty acid content related to intrinsic aging. However, their intensity is decreased in the hand samples when compared to the corresponding arm samples, indicating a decrease in these molecules related to UV exposure and photoaging effects. As previously mentioned, various trends in ion intensity could be identified within the data (Figure 3a) which validates that the differences seen are physiologically relevant and not experimental artefacts.

Another ion that could be easily identified was the $[M-H]^-$ molecular marker of cholesterol sulfate with m/z = 465. This ion demonstrated both high reliability as a biomarker and a high contribution to class variance in the loadings plot relating to the post-menopausal body site comparison (Figure 2b). However, it also proved to have a good reliability ($0.5<p(corr)[1]<-0.5$) (Figure S3) for all of the other comparisons except the under 27 body site (Figure 2d) and demonstrated a statistically significant difference in peak intensity between all classes (p value <0.001). The change in the presence of this molecule is particularly interesting because, as mentioned previously, this molecule is present at low levels within the *SC* but has been shown to play a key role in regulating desquamation.

Changes in the intensity of this ion can be clearly observed through visual inspection of the spectra, as illustrated in Figure 3b. Figure 3c shows the average normalised intensities for the cholesterol sulfate ion peak for all classes. A statistically significant difference between the classes in all four comparisons was demonstrated using a student's t-test. The intensity of this ion is increased in both the post-menopausal samples compared to the under 27 samples and in the hand samples compared to the corresponding arm samples, showing an increase in cholesterol sulfate related to both intrinsic and extrinsic aging. The extrinsic aging difference is more significant in the post-menopausal volunteers compared to the under 27 year olds, which is proposed to be due to an accumulation effect caused by prolonged UV exposure. A change in the concentration of cholesterol sulfate due to aging has been demonstrated in murine skin[25] but has not previously been reported for human *SC* analysis. However, it does correlate to what is currently known about this molecule, whereby an increase in cholesterol sulfate has been associated with diseases that cause heightened desquamation, producing symptoms of scaly and peeling skin. These symptoms are also commonly seen with both elderly skin and skin which has suffered prolonged UV exposure.

It is important to note that two different body sites are being compared in order to assess possible extrinsic aging and therefore inherent differences in the *SC* composition due to body location cannot be ruled out. Ideally, analysis would be conducted on the same body site before and after acute UV exposure. However, this is not a viable option when conducting *in vivo* sampling on human volunteers. A comparison between other body locations, such as the buttock and face, would have provided a more extreme comparison of UV exposure effects. However, this may have produced a more significant difference in *SC* composition due to location. Therefore, the two body sites chosen for comparison were a compromise between a difference in UV exposure and a similarity in body location. If the differences observed were solely an effect of body site and not UV exposure then a similar variance between the sites would be expected for both age groups. However, the difference in cholesterol sulfate levels between the two body sites is much greater for the post-menopausal volunteers, indicating an accumulative effect caused by prolonged UV exposure over time.

The presence of cholesterol sulfate was also monitored as a function of depth for each sample type. Figure 3d shows the normalised intensity for this ion as a function of tape strip number from an example data set. It is important to note that as this data is only taken from one volunteer per age category it does not accurately represent the average trends between sample types seen in Figure 3c. However, it does demonstrate an increase in the level of cholesterol sulfate with increasing *SC* depth, with a statistically significant increase seen in all sample types between tape strip 1 and 15. This finding agrees with already established knowledge that there is a cholesterol sulfate gradient which reaches a maximum in the deeper layers of the *SC*, but decreases abruptly in the superficial layers.[35]

The effects of aging on cholesterol sulfate distribution within the *SC*. The 2D distribution of cholesterol sulfate within a single tape stripped layer was also examined by mapping the cholesterol sulfate $[M-H]^-$ molecular ion ($C_{27}H_{45}SO_4^-$). Figure 4a illustrates a representative ToF-SIMS secondary ion image for tape strip 7 for each sample type.

The intensity of the $C_{27}H_{45}SO_4^-$ ion in these secondary ion images confirms the previously reported trend that cholesterol sulfate levels are increased as a result of both intrinsic and photoaging. However, a more interesting observation, and one that cannot be highlighted by the spectra alone, is the non-uniform distribution of this molecule. These images, particularly those from the post-menopausal age group, demonstrate a localised increase in this molecule shown by "pools" of higher ion intensity. This suggests that the age-induced increase in cholesterol sulfate within the *SC* is a non-uniform process, initially affecting isolated areas rather than a homogeneous increase. The distribution of the fatty acid lignoceric acid (C24:0) has also been presented in Figure 4a to demonstrate that although there is a change in intensity in this lipid between sample groups it appears to be uniform across the tissue. This supports the suggestion that the localisation effect of cholesterol sulfate is the result of a physiological effect and not an artefact of the data. This localised effect can also be observed when assessing the spatial distribution as a function of *SC* depth. Figure 4b shows the ToF-SIMS secondary ion images for cholesterol sulfate for various strip numbers for the arm and hand samples of one post-menopausal volunteer. These images highlight that the localised increase in cholesterol sulfate seen in the tape strip 7 samples is actually present throughout the *SC*. This effect is most pronounced for the post-menopausal hand samples which even show "pools" of increased cholesterol sulfate in the outermost layer (strip 1). The fact that this localisation is present in multiple layers of the *SC* confirms that it is the result of a non-uniform physiological change in cholesterol sulfate levels.

CONCLUSIONS

This work demonstrates successful analysis of human *SC* lipids from individual tape stripped samples using ToF-SIMS. This technique identified a statistically significant increase in cholesterol sulfate relating to both intrinsic and extrinsic aging, a molecule which has not previously been linked to aging of human skin. The imaging capabilities of ToF-SIMS also highlighted a varied spatial distribution and apparent localised increase in this sterol within an individual tape stripped layer, a finding which proved consistent throughout the *SC*. Age related changes in the prevalence of two abundant fatty acids, lignoceric and hexacosanoic acid, were also observed. Importantly, all chemical changes were detected from native samples collected *in vivo* from human volunteers.

In order to support the chemical changes detected, established surface analysis techniques, SEM and AFM were employed to assess physical changes within our samples. SEM identified previously reported age-related changes to corneocyte morphology within the individual tape stripped layers, validating the chemical age-related changes seen at this level. The AFM analysis confirmed that an equal depth of *SC* was being removed per sample type, which confirmed that the chemical differences seen were the result of a physiological change and not due to a difference in the depth of *SC* analysed.

Previously unreported age-related changes to human *SC* have been described, which offer insight into mechanisms of aging relevant to both the pharmaceutical and cosmetic industries. The technique could also easily be applied to monitor other changes to human *SC* as a function of depth, such as physiological effects relating to race, gender, disease etc. or the alternatively the permeation of xenobiotic substances.

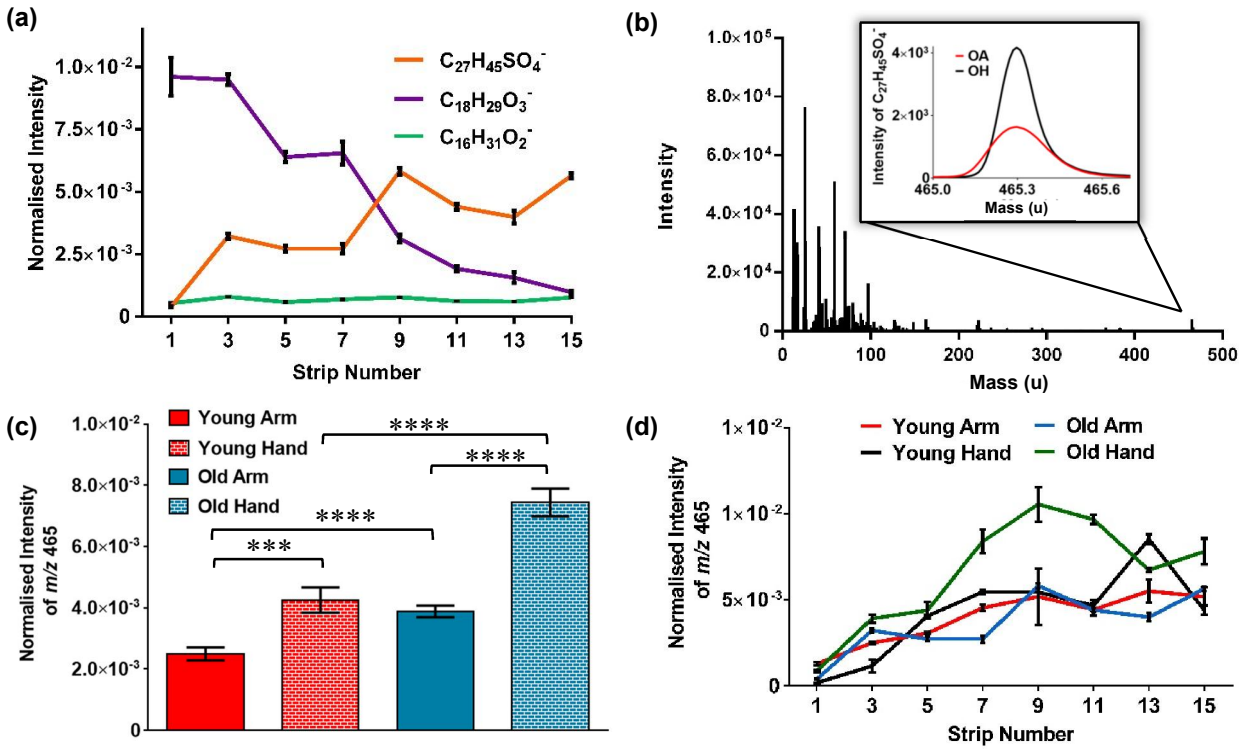

Figure 3. (a) ToF-SIMS secondary ion intensities (normalised to total ion counts) for one post-menopausal volunteer arm sample, illustrating the presence of various trends in ion intensity as a function of *SC* depth. (b) An example ToF-SIMS spectrum of a tape stripped human *stratum corneum* sample, highlighting the cholesterol sulfate $[M-H]^-$ peak at $m/z = 465$. The inset shows the difference in normalised intensity for the cholesterol sulfate negative molecular ion peak seen in the spectra of a post-menopausal arm and hand sample. (c) ToF-SIMS secondary ion intensities (normalised to total ion counts) for the cholesterol sulfate ion peak across the four sample types. The data is shown as the mean and standard error calculated from tape strip number 7 for n= 9 volunteers per sample type and n = 4 measurements per sample. An unpaired, two tailed T test with Welch's correction was conducted on each sample pair (**** p value < 0.0001, *** p value <0.001). (d) ToF-SIMS secondary ion intensities (normalised to total ion counts) for the cholesterol sulfate ion peak as a function of tape strip depth. Data was taken from alternate strips between 1 and 15 for one volunteer per age category. An unpaired, two tailed T test with Welch's correction was conducted on tape strip 1 and 15 for each sample type and all showed a significant increase (p value <0.01).

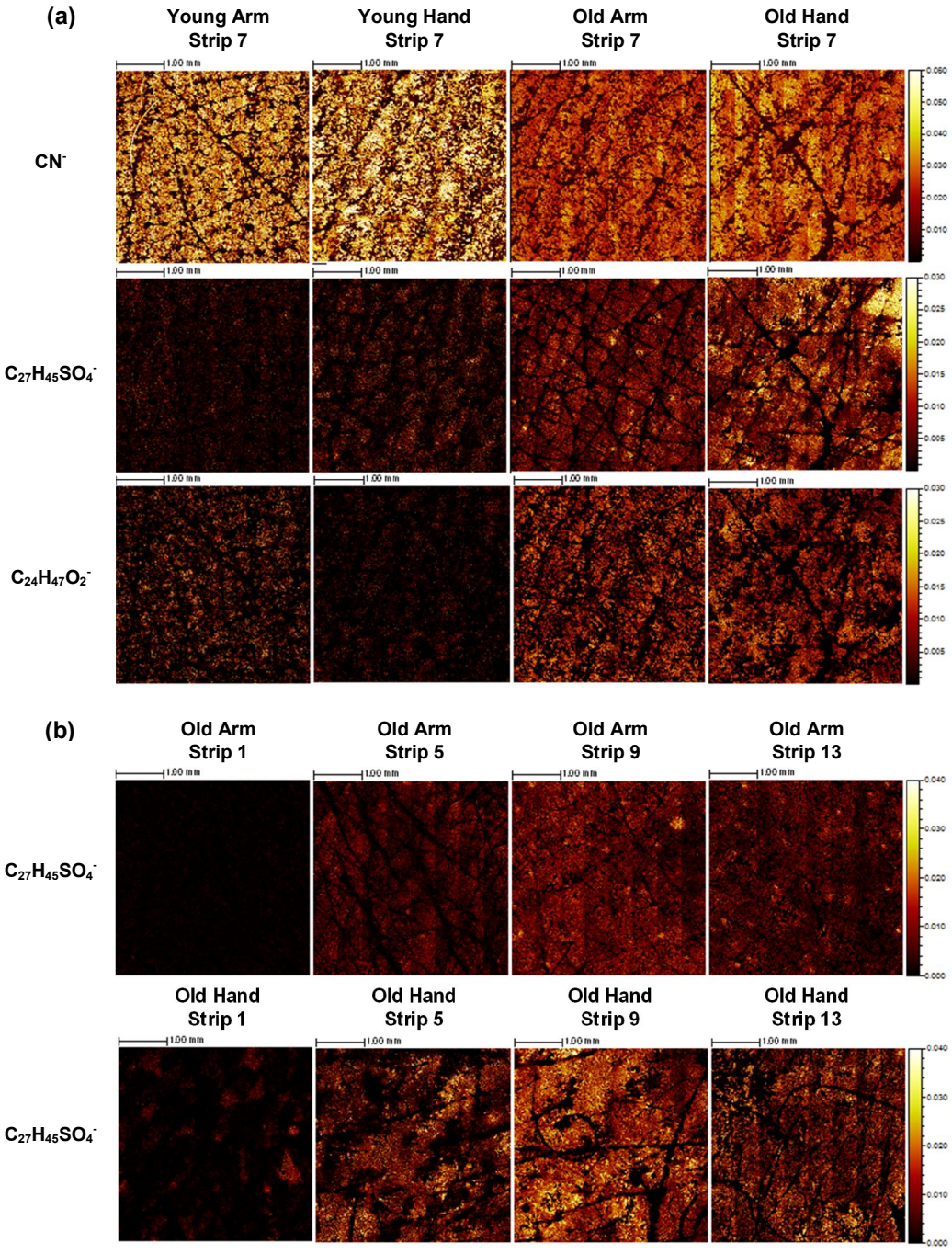

Figure 4. ToF-SIMS 4 × 4 mm secondary ion distribution maps. The scale bar represents 1 mm and the images have been normalised to the total ion image. (a) Example distribution maps from one volunteer per age group, tape strip number 7 showing the distribution of the generic tissue marker (CN^-), the cholesterol sulfate molecular ion ($C_{27}H_{45}SO_4^-$) and lignoceric acid ($C_{24}H_{27}O_2^-$). (b) Example secondary ion maps from one post-menopausal volunteer showing the distribution of the cholesterol sulfate molecular ion ($C_{27}H_{45}SO_4^-$) across various tape strip numbers.

ASSOCIATED CONTENT

Supporting Information

The Supporting Information is available free of charge on the ACS Publications website.

Individual strip AFM data, PCA score plots of ToF-SIMS data, ToF-SIMS OPLSDA S-plot data, ToF-SIMS peak intensities for lignoceric and hexacosanoic acid. (PDF)

AUTHOR INFORMATION

Corresponding Author

* David.Scurr@nottingham.ac.uk

ACKNOWLEDGMENT

The authors would like to thank all of the funding bodies for their contributions: The University of Nottingham Centre for Doctoral Training in Targeted Therapeutics and Formulation Science, Walgreens Boots Alliance and EPSRC (Grant EP/I01375X/1). Special thanks to Christine Grainger-Boultby for her SEM expertise. All relevant data can be accessed through the Nottingham Research Data Management Repository at http://dx.doi.org/10.17639/nott.42.

REFERENCES

(1) van Smeden, J.; Janssens, M.; Gooris, G. S.; Bouwstra, J. A. *Biochim. Biophys. Acta, Mol. Cell Biol. Lipids* **2014**, *1841*, 295-313.

(2) Elias, P. M.; Feingold, K. R.; Denda, M. In *Dermal Absorption and Toxicity Assessment,* 2nd ed.; Roberts, M. S., Ed.; CRC Press, **2007**, 79-87.

(3) Harding, C. R. *Dermatol Ther.* **2004**, *17 Suppl 1*., 6-15.

(4) Jungersted, J. M.; Agner, T. *Contact Dermatitis* **2013**, *69*, 65-71.

(5) Neunzehn, J.; Draude, F.; Golla-Schindler, U.; Arlinghaus, H. F.; Wiesmann, H. P. *Surf. Interface Anal.* **2013**, *45*, 1340-1346.

(6) Sjovall, P.; Rossmeisl, M.; Hanrieder, J.; Kuda, O.; Kopecky, J.; Bryhn, M. *Anal. Bioanal. Chem.* **2015**, *407*, 5101-5111.

(7) Wehrli, P. M.; Lindberg, E.; Angerer, T. B.; Wold, A. E.; Gottfries, J.; Fletcher, J. S. *Surf. Interface Anal.* **2014**, *46*, 173-176.

(8) Passarelli, M. K.; Newman, C. F.; Marshall, P. S.; West, A.; Gilmore, I. S.; Bunch, J.; Alexander, M. R.; Dollery, C. T. *Anal. Chem.* **2015**, *87*, 6696-6702.

(9) Hanrieder, J.; Malmberg, P.; Lindberg, O. R.; Fletcher, J. S.; Ewing, A. G. *Anal. Chem.* **2013**, *85*, 8741-8748.

(10) Lazar, A. N.; Bich, C.; Panchal, M.; Desbenoit, N.; Petit, V. W.; Touboul, D.; Dauphinot, L.; Marquer, C.; Laprevote, O.; Brunelle, A.; Duyckaerts, C. *Acta Neuropathol.* **2013**, *125*, 133-144.

(11) Judd, A. M.; Scurr, D. J.; Heylings, J. R.; Wan, K. W.; Moss, G. P. *Pharm. Res.* **2013**, 30, 1896-1905.

(12) Kezutyte, T.; Desbenoit, N.; Brunelle, A.; Briedis, V. *Biointerphases* **2013**, *8*, 1-8.

(13) Lampe, M. A.; Burlingame, A. L.; Whitney, J.; Williams, M. L.; Brown, B. E.; Roitman, E.; Elias, P. M. *J. Lipid Res.* **1983**, *24*, 120-130.

(14) Elias, P. M.; Williams, M. L.; Choi, E. H.; Feingold K. R. *Biochim. Biophys. Acta, Mol. Cell Biol. Lipids* **2014**, *1841*, 353–361.

(15) Sato, J.; Denda, M.; Nakanishi, J.; Nomura, J.; Koyama, J. *J. Invest. Dermatol.* **1998**, *111*, 189-193.

(16) Williams, M. L.; Elias P. M. *J. Clin. Invest.* **1981**, 68, 1404-10.

(17) Elias, P.M.; Williams, M. L.; Maloney, M. E.; Bonifas, J. A.; Brown, B. E.; Grayson, S.; Epstein, EH Jr. *J. Clin. Invest.* **1984**, *74*, 1414-21.

(18) Farage, M. A.; Miller, K. W.; Maibach, H. I. *Textbook of Aging Skin*, Springer Science & Business Media, **2009**, 129.

(19) Luebberding, S.; Krueger, N.; Kerscher, M. *Int. J. Cosmet. Sci.* **2013**, *35*, 183-190.

(20) Imokawa, G.; Abe, A.; Jin, K.; Higaki, Y.; Kawashima, M.; Hidano, A. *J. Invest. Dermatol.* **1991**, 96, 523-526.

(21) Rogers, J.; Harding, C.; Mayo, A.; Banks, J.; Rawlings, A. *Arch. Dermatol. Res.* **1996**, *288*, 765-770.

(22) Denda, M.; Koyama, J.; Hori, J.; Horii, I.; Takahashi, M.; Hara, M.; Tagami, H. *Arch. Dermatol. Res.* **1993**, *285*, 415-417.

(23) Bak, H.; Hong, S. P.; Jeong, S. K.; Choi, E. H.; Lee, S. E.; Lee, S. H.; Ahn, S. K. *Int. J. Dermatol.* **2011**, *50*, 832-837.

(24) Boireau-Adamezyk, E.; Baillet-Guffroy, A.; Stamatas, G. N. *Skin Res. Technol.* **2014**, *20*, 409-415.

(25) Haratake, A.; Komiya, A.; Horikoshi, T.; Uchiwa, H.; Watanabe, S. *Skin Pharmacol. Physiol.* **2006**, 19, 275-82.

(26) Bonte, F.; Saunois, A.; Pinguet, P.; Meybeck, A. *Arch. Dermatol. Res.* **1997**, *289*, 78-82.

(27) Egawa, M.; Tagami, H. *Br. J. Dermatol.* **2008**, *158*, 251-260.

(28) Fitzpatrick, T. B. *Arch. Dermatol.* **1988**, *124*, 869-871.

(29) Graham, D. J.; Castner, D. G. *Biointerphases* **2012**, 7, 1-12.

(30) Triba, M. N.; Le Moyec, L.; Amathieu, R.; Goossens, C.; Bouchemal, N.; Nahon, P.; Rutledge, D. N.; Savarin, P. *Mol. BioSyst.,* **2015**, *11*, 13-19.

(31) Picardo, M.; Ottaviani, M.; Camera, E.; Mastrofrancesco, A. *Derm.-Endocrinol.* **2009**, *1, 68-71.*

(32) Pochi, P. E.; Strauss, J. S.; Downing, D. T. *J. Invest. Dermatol.* **1979**, *73*, 108-111.

(33) Worley, B.; Powers, R. *Curr. Metabolomics* **2013**, 1, 92–107

(34) Norlén, L.; Nicander, I.; Lundsjö, A.; Cronholm, T.; Forslind, B. *Arch. Dermatol. Res.* **1998**, *290*, 508-516.

(35) Bouwstra, J. A.; Gooris, G. S.; Dubbelaar, F. E. R.; Ponec, M. *J. Lipid Res.* **1999**, *40*, 2303-2312.